

HEPA FILTER MATERIAL LOAD DETECTION USING A MICROWAVE CAVITY SENSOR

A. Mason¹, S. Wylie¹, A. Thomas², H. Keele², A. Shaw¹ and A.I.Al-Shamma'a¹

¹School of Built Environment, Liverpool John Moores University, Liverpool, L3 2ET, UK.

²Dstl, Porton Down, Salisbury, SP4 0JQ, UK.

Email: a.mason1@ljmu.ac.uk

Abstract- This paper presents a novel microwave cavity sensor application for the detection of HEPA filter particulate loading. The sensor resonates at 3.435GHz and 8.570GHz when empty, where the TM_{010} and TM_{020} modes dominate respectively. Experimental results show that the resonant frequency of the sensor shifts significantly when filters of different particulate loadings are presented to it. This is a significant finding, and means that the sensor could present an effective solution for determining the loading of periodic use HEPA filters (e.g. those used in personal respirators), which are often disposed of unnecessarily.

Index terms: HEPA filter, filter load, filter ageing, filter sensor, microwave cavity, microwave sensor.

I. INTRODUCTION

High Efficiency Particulate Air (HEPA) filters are typically employed for particle removal and retention in air cleaning systems. These are commonly used in clean rooms in the pharmaceutical, nuclear and semiconductor industries [1, 2]. Such filters also have practical applications for military purposes, and have their roots as far back as the Manhattan Project [3]. Figure 1 shows an example of a personal respiratory aid which makes use of HEPA filters. Regardless of the application, the main objectives of HEPA filters are to either prevent contamination of sensitive products with airborne particles, or to protect people from dangerous micro-organisms and germs by ensuring that the filtered air possesses a defined degree of sterility [4].



Figure 1. A respiratory device with two HEPA filters, designed to protect the user from inhaling particulates.

HEPA filters are typically made from fibreglass strands which are $0.5\text{-}2\mu\text{m}$ in diameter. These fibres are randomly arranged, and have the ability to capture particles which are smaller than the air gaps between the fibres. Three main mechanisms occur to prevent particulates penetrating – these are:

- 1) **Diffusion** – particles collide causing their path through the filter to be impeded, this leads to an increased probability of the following two mechanisms being effective.
- 2) **Interception** – particles following the air flow pass very close to a fibre, therefore adhering to it.
- 3) **Impaction** – particles which are too large to follow the air flow through the filter are forced to embed themselves within the filter.

Diffusion is particularly effective for the capture of very small particles ($< 0.1\mu\text{m}$ diameter), whilst impaction is most effective for coarser particles. Table 1 gives an indication of the sizes of particulates that HEPA filters might be expected to capture. Figure 2 shows an image of how the fibres might be arranged when viewed with a SEM [5].

Table 1: Sizes of materials that a HEPA filter might encounter during active use.

Particle	Particle diameter (μm)
Viruses	0.003-0.06
Bacteria	0.4 – 5
Fungal spores	2-10
Pollen grain	10-100
Dust	< 100



Figure 2. How the filter might appear when viewed with a SEM [5].

Over the filter lifetime, deposits build up on the fibres – these deposits are often referred to as particle cakes [2, 5-8]. These deposits have two effects, the first of which is to initially increase the efficiency of the filter, since the captured particulate matter begins to settle on the filter and block further particles from passing. The second effect is for the filter to become clogged, which leads to a drop in air pressure after the filter due to the impedance of air flow. It is this change in pressure that is commonly detected using two pressure transducers [1, 4, 6, 9, 10], one either side of the filter, to detect when a filter requires cleaning or replacement. In many situations, particularly where air flow is continuous (e.g. air conditioning or clean room filtration), this is a perfectly adequate solution. However there are situations where this manner of detection is not appropriate, such as with the use of portable respiratory devices or protective garments. In both of these cases use is periodic and so the filter may be loaded partially when stored, even if there is little or no air flow. As a result, the device requires testing before reuse, but since there is

currently no convenient method permitting the residual life or capacity of such devices to be determined, a conservative filter change policy leads to disposal of filters which are not necessarily expired. The result of this is significant wastage of usable filters which is both costly and unnecessary, which leads to the purpose of this work: to find a filter sensing technique which does not require air flow in order to determine remaining filter capacity. This is important for personal breathing apparatus where users respiratory system may be unprotected during the time it takes for a differential pressure sensor to determine the condition of the filter.

II. THEORY

An alternative to differential pressure measurement is to consider the change in relative permittivity (ϵ_r) of the filter material. The filter, when clean, will have an average ϵ_r which will change as it becomes loaded with particulate matter. One method which can be used to find the ϵ_r of a substance is to monitor the effect it has on the resonant frequencies of an electromagnetic (EM) cavity. An EM cavity, consisting of a hollow structure with conducting walls, will resonate when it is excited at an appropriate frequency by a small antenna placed inside the structure. The resonant modes occur when the electric and magnetic fields form standing waves, and so depend upon the internal dimensions of the cavity and the permittivity of any material placed inside. For a cylindrical cavity based sensor the fundamental modes are TE_{111} and TM_{010} . TE (Transverse Electric) Modes have a magnetic component in the propagation direction and TM (Transverse Magnetic) Modes have an electric component in the propagation direction. Each mode will generate a resonant peak with a quality factor (Q), which is inversely proportional to the power dissipated in the cavity for each applied EM oscillation. A high Q indicates a sharp resonant peak that will be more readily analysed and improve the accuracy of the sensor.

The resonant frequency for TE_{nml} and TM_{nml} modes in a cylindrical cavity [11] can be calculated using equation (1).

$$f_{nml} = \frac{c}{2\pi\sqrt{\mu_r\epsilon_r}} \left[\left(\frac{p_{nm}}{a} \right)^2 + \left(\frac{l\pi}{d} \right)^2 \right]^{1/2} \quad (1)$$

Where:

c is the speed of light

μ_r is of the relative permeability

ϵ_r is the relative permittivity

p_{nm} is the m^{th} root of the of Bessel function of the n^{th} order for TM modes

or the m^{th} root of the first derivative of Bessel function of the n^{th} order for TE modes

a is the radius of the cavity

d is the depth of the cavity

All EM modes therefore have the same dependence upon $\sqrt{\epsilon_r}$, so when the cavity is excited by an appropriate range of frequencies and the resulting spectrum is captured, the resonant peaks corresponding to these modes will shift to lower frequencies as the permittivity is increased.

The HEPA filter material used in the experimentation was approximately 0.5mm thick and had a diameter of 120mm. To this end, a so called pancake cavity was created, which comprised two aluminium discs placed (rather than fixed) one on top of the other. Each has a counter bored hole of diameter 60mm and depth 3mm, to create an internal cavity which is 6mm deep. Externally, N-type panel connectors with 5mm probes are used to allow the passage of microwave energy into and out of the cavity. The cavity was modelled in the Ansoft HFSS package [12] as shown in Figure 3, with the physical cavity pictured in Figure 4. Figures 5 and 6 show a comparison of the simulated and measured power for reflection and transmission respectively.

The simulated and measured data shows that resonance occurs at 3.825GHz and 8.570GHz when considering the range 1-10GHz. Using equation (1), these resonances represent the modes TM_{010} and TM_{020} respectively, and are presented graphically in Figure 7. The design of the sensor is such that it allows rapid testing of the filter materials – inserting a filter for testing is simply a matter of sandwiching the material between the two aluminium discs. This does alter the depth of the cavity but due to the slimness of the HEPA filter little change in performance occurs, mainly since TM_{010} and TM_{020} are not depth dependant.

There is some discrepancy in the measured and simulated signal magnitudes which is largely due to noise in the case of transmission; however there is good agreement for the points at which resonance occurs.

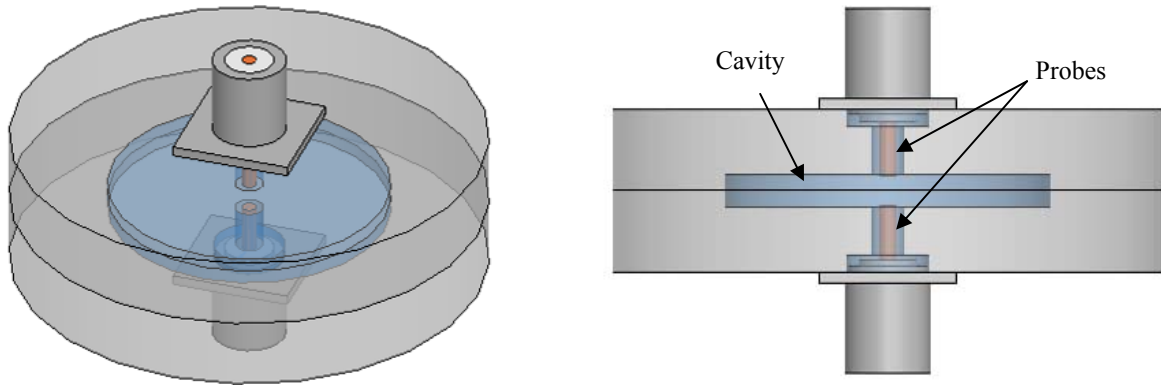


Figure 3. Ansoft's HFSS [12] modelling software showing the design structure of the resonant cavity used in this work. The left image displays a more complete view of the cavity, whilst the image on the right shows a side view, which clearly shows the cavity part of the sensor.

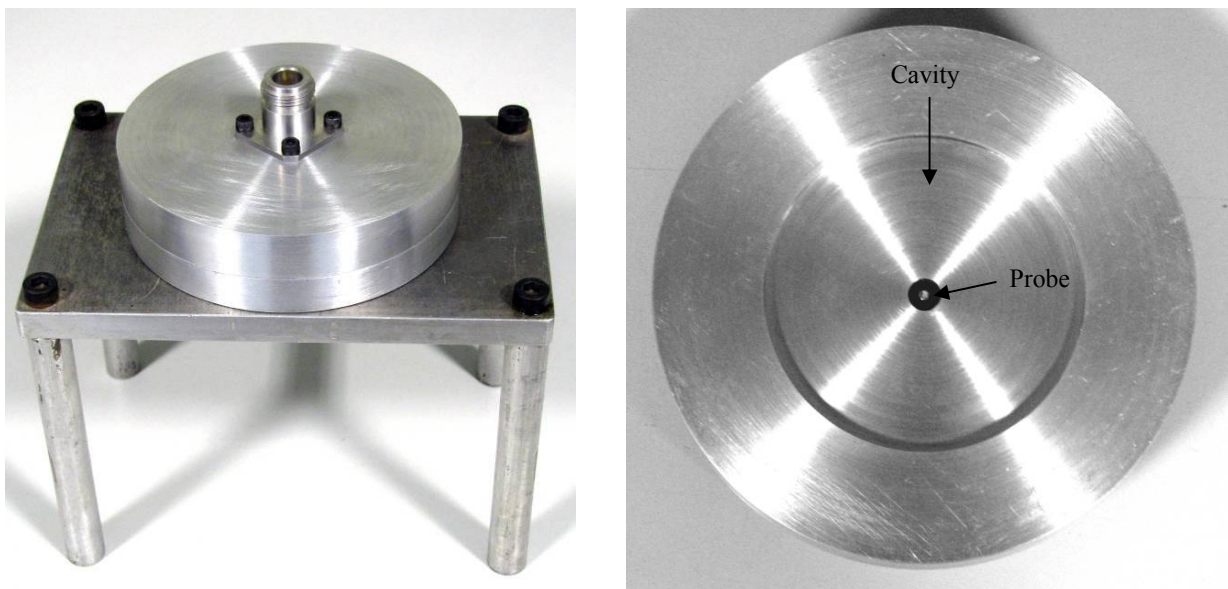


Figure 4. The cavity post production, using the same dimensions as those modelled in Ansoft HFSS. The left image shows the sensor in its useable state and on a purpose made stand for stability, whilst the image on the right shows a single disc of the sensor, displaying half of the shallow cavity and a probe feed.

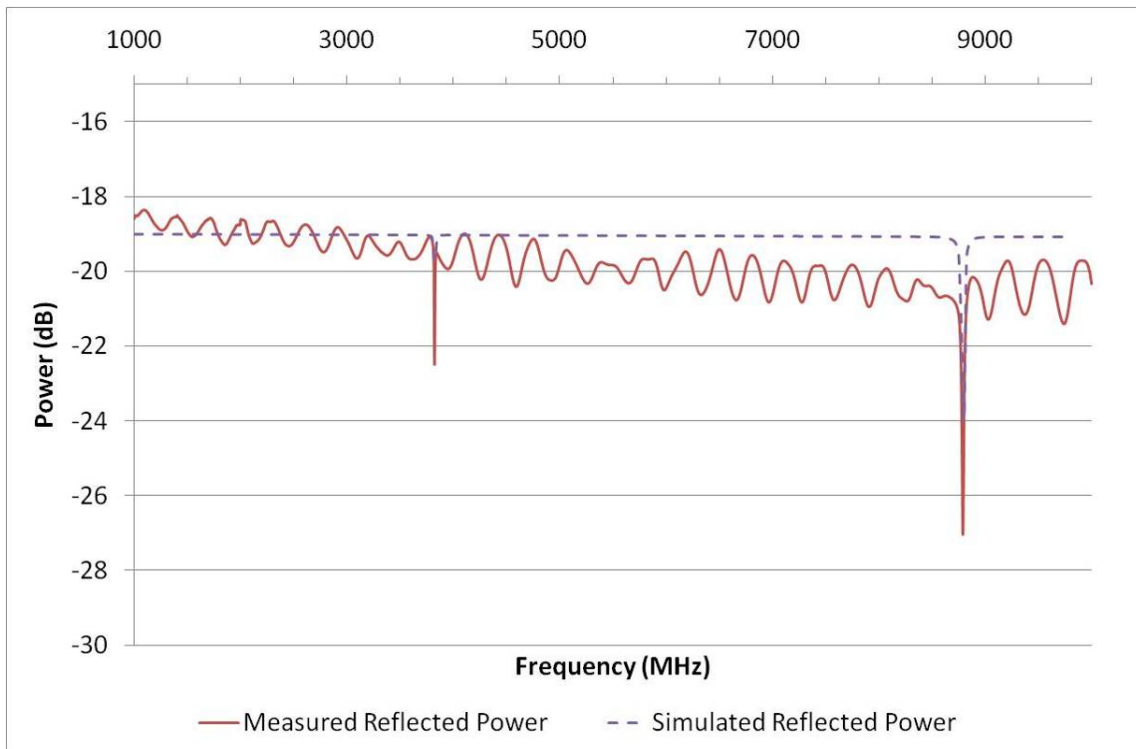


Figure 5. Comparison of the modelled and measured reflected power from the sensor.

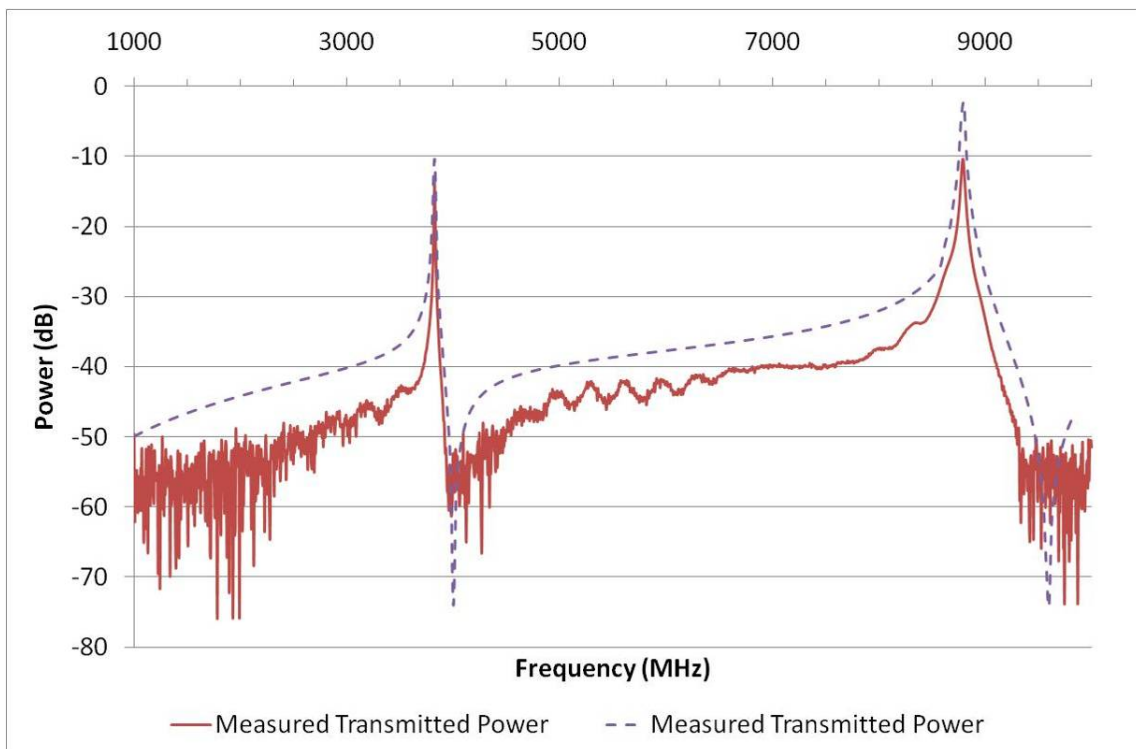


Figure 6. Comparison of the modelled and measured transmitted power through the sensor.

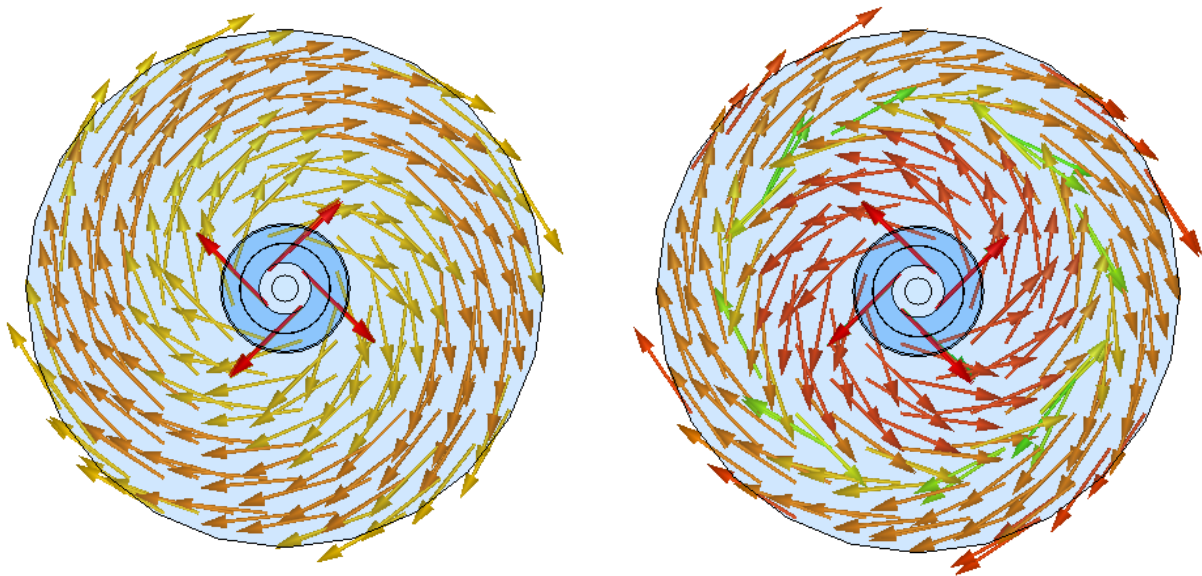


Figure 7. A top view of the cavity volume showing the magnetic field vectors for the TM₀₁₀ (left) and TM₀₂₀ (right) modes, which occur at 3.835GHz and 8.570GHz respectively.

III. EXPERIMENTAL SETUP

a. Filter material preparation

Five filters were prepared for comparison by the cavity sensor. A standard test dust was used to load four of the filters (samples A-D) such that they trapped different weights of the dust; these weights were determined by the percentage of air flow allowed by the filter during loading. The final filter (sample E) received no loading and was labelled as the clean sample, representing an unused filter. The test dust used in the experimentation was BS1701 coarse dust, which is a standard test dust with particles ranging from 0-150 μ m and being made from quartz flour. This dust exceeds the size of most real world particulates that a filter would be expected to remove, but also meant that the filters were saturated relatively quickly via impaction for experimental purposes. Table 2 shows the weight of the dust held by each of the filters after loading and the amount of air allowed to pass through the filter as a result. The samples were promptly sealed in polyethylene bags to prevent dust escaping before testing with the cylindrical cavity sensor.

Table 2: Weight of the dust held by each filter sample and the percentage of air allowed through the filter after loading.

Sample name	Air allowed to flow (%)	Weight of dust held (g)
A	0	4.70
B	25	3.29
C	50	1.04
D	75	0.67
E	100	0

b. Data acquisition

The equipment used for data acquisition is shown in Figure 8. The cavity was connected to a Marconi 6200A microwave test set, using a Wiltron Autotester to allow reflected power measurement, and a Marconi 6230A Scalar Detector to measure transmitted power. The filters were left in their polyethylene bags so that the dust particles were not disturbed or lost during testing. The Marconi test set was connected via a GPIB interface to a PC, which ran a bespoke C# application allowing data capture and presentation. The software interface is shown in Figure 9. The software allows high resolution data capture by joining results from discrete frequency intervals – this overcomes the 1601 data point per sweep limitation of the test set. The software was set to operate between 1 and 10GHz, with 1GHz intervals. Each filter was sampled 6 times and their results (shown later) represent an average of these samples.

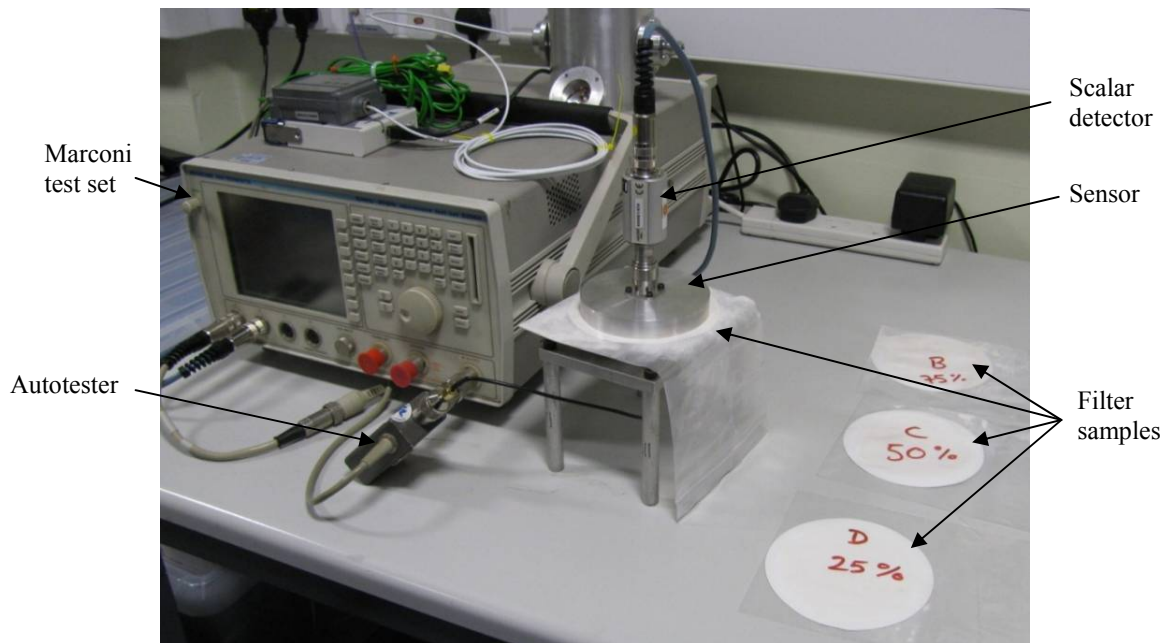


Figure 8. Experimental setup showing the sensor connected to a Marconi 6200A microwave test set and holding a filter material sample.

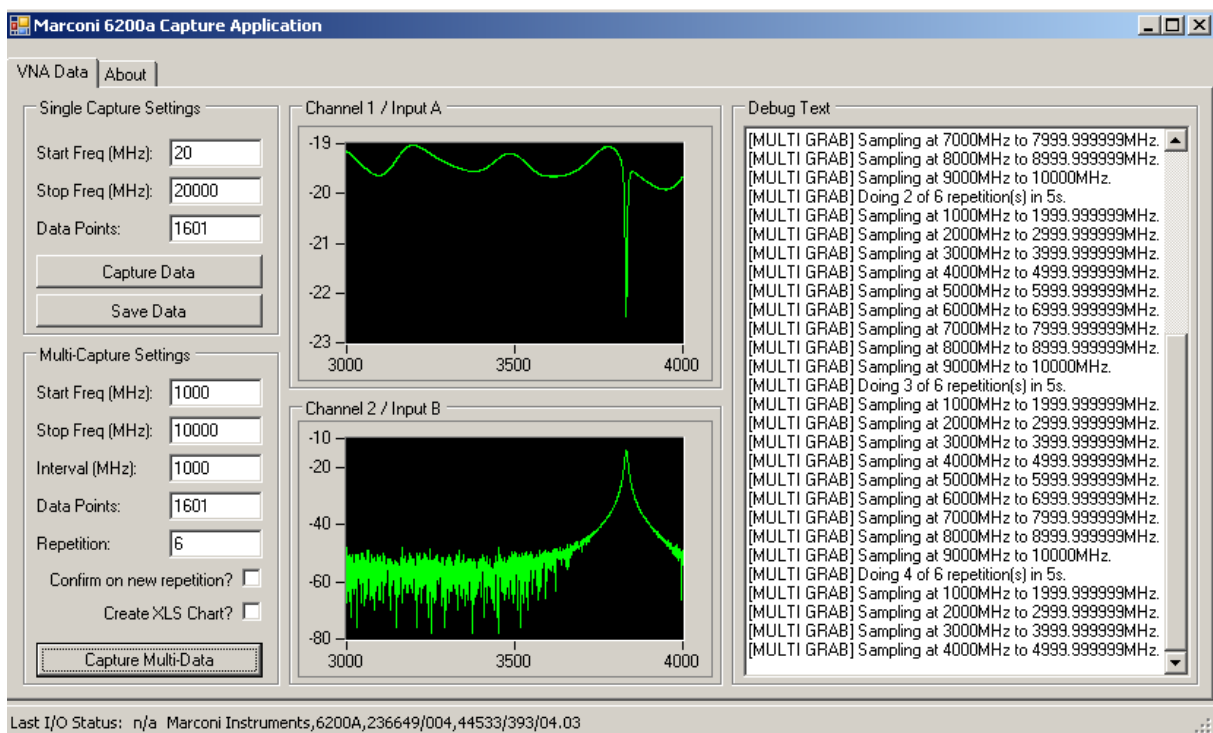


Figure 9. Bespoke C# application for acquiring and presenting data from the Marconi 6200A microwave test set.

IV. RESULTS

Experimental results from testing the filter material in the sensor are shown in Figures 9-14. Figures 10-12 show results for reflected power and Figures 13-15 show results for transmitted power. Figures 11, 12, 14 and 15 show the most significant changes in the spectral data, which occur at the points where the TM_{010} and TM_{020} modes are dominant. Table 3 includes information regarding the frequency at which peaks occur, as well as the change which occurs as a result of the different filter loadings.

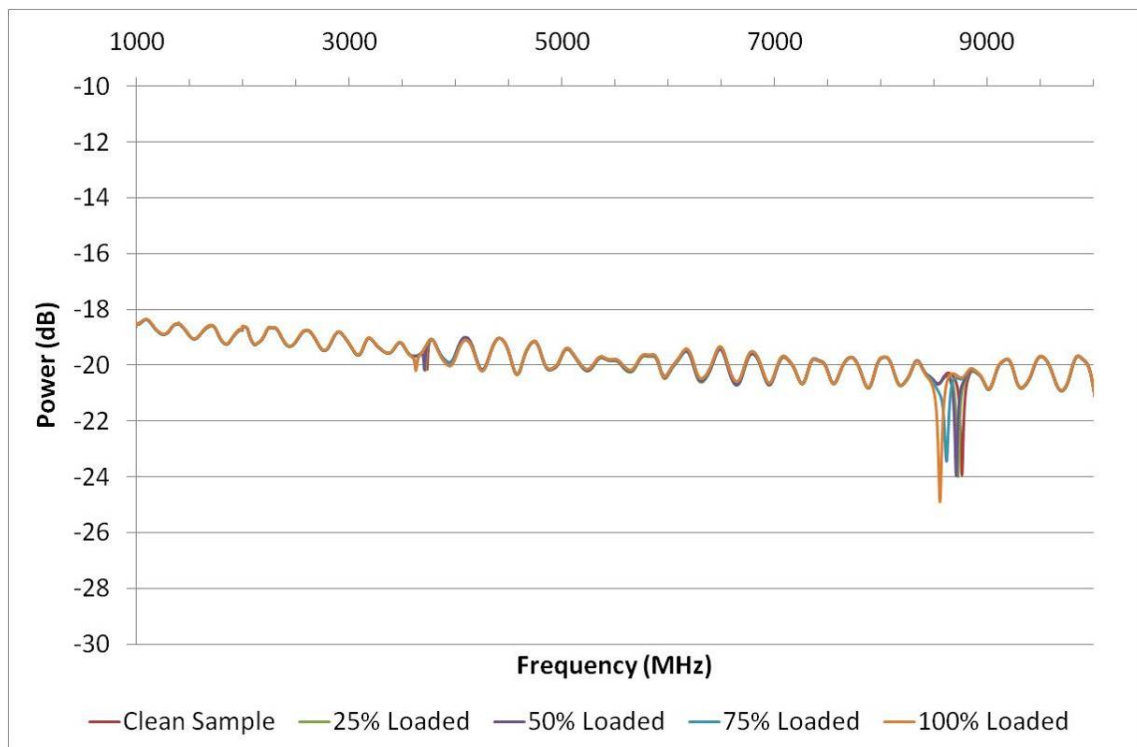


Figure 10. Spectral data for reflected power in the range 1-10GHz, showing two distinct areas of interest at the resonant peaks.

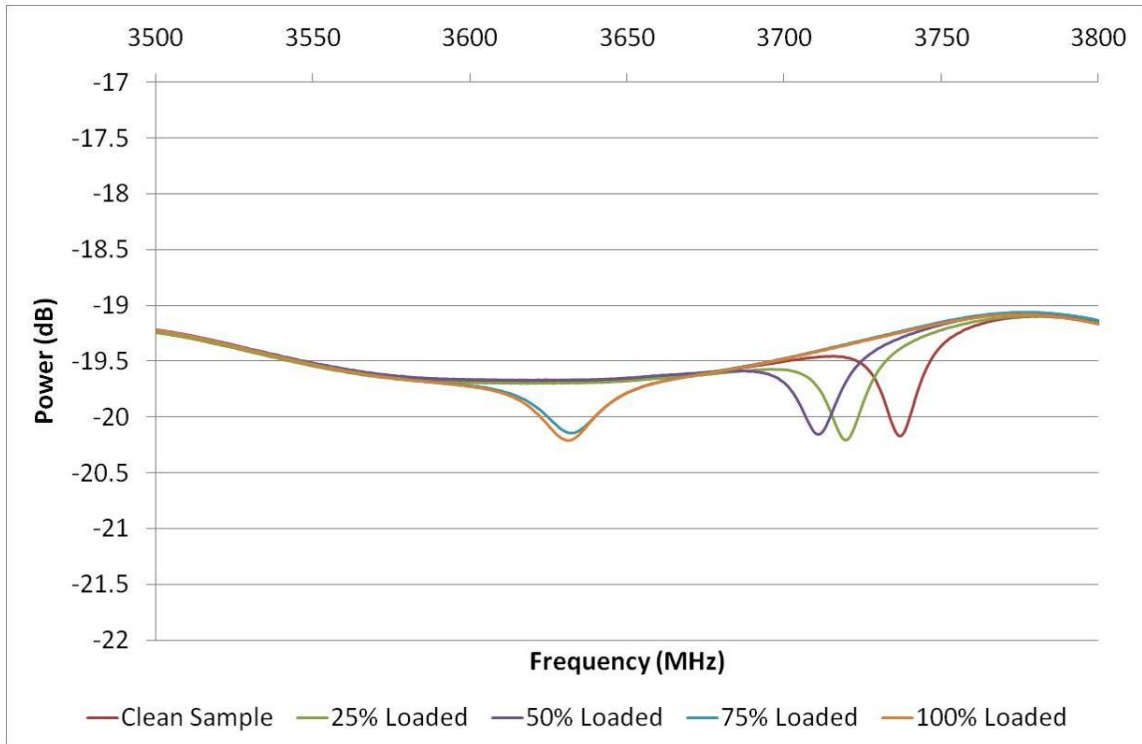


Figure 11. Spectral data for reflected power in the range 3.5-3.8GHz, showing resonant peak shifts dependant on filter loading.

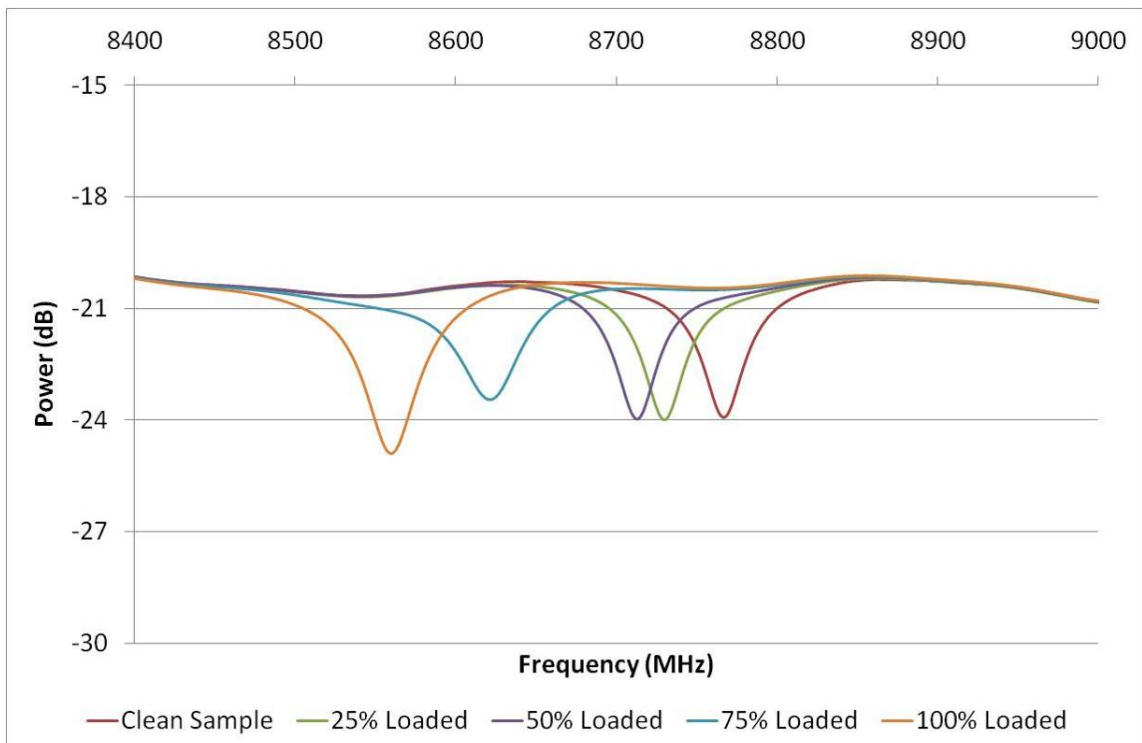


Figure 12. Spectral data for reflected power in the range 8.4-9.0GHz, showing resonant peak shifts dependant on filter loading.

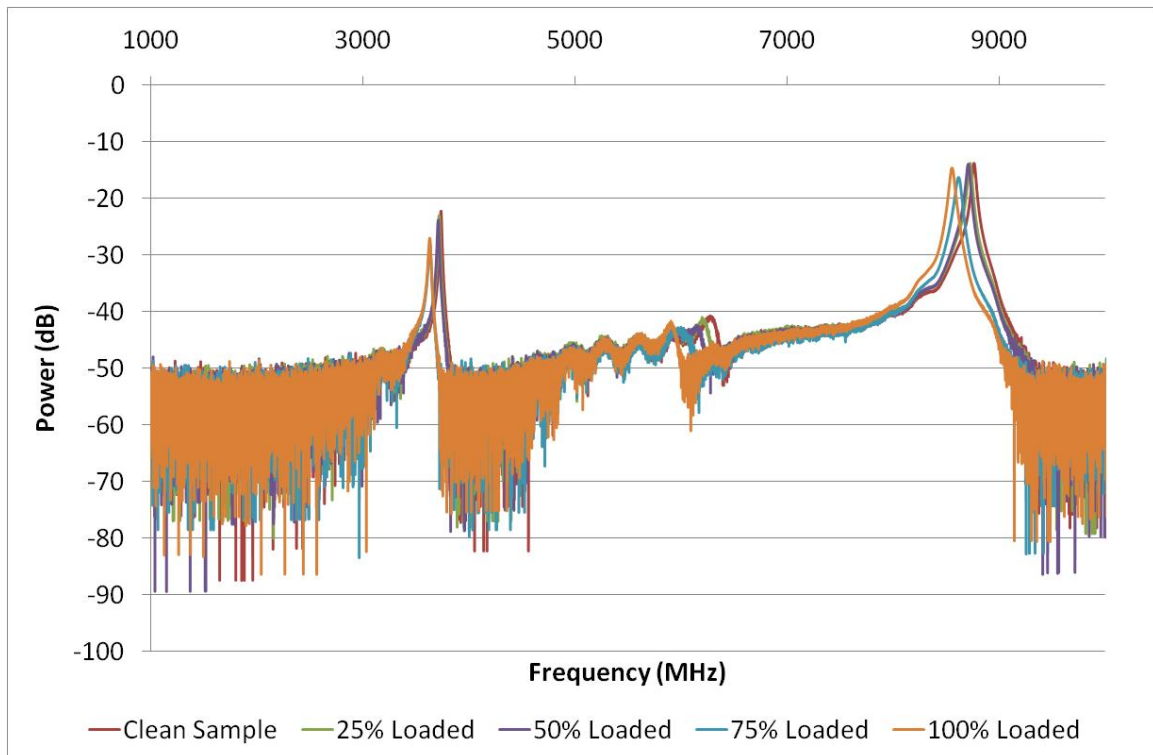


Figure 13. Spectral data for transmitted power in the range 1-10GHz, showing two distinct areas of interest at the resonant peaks.

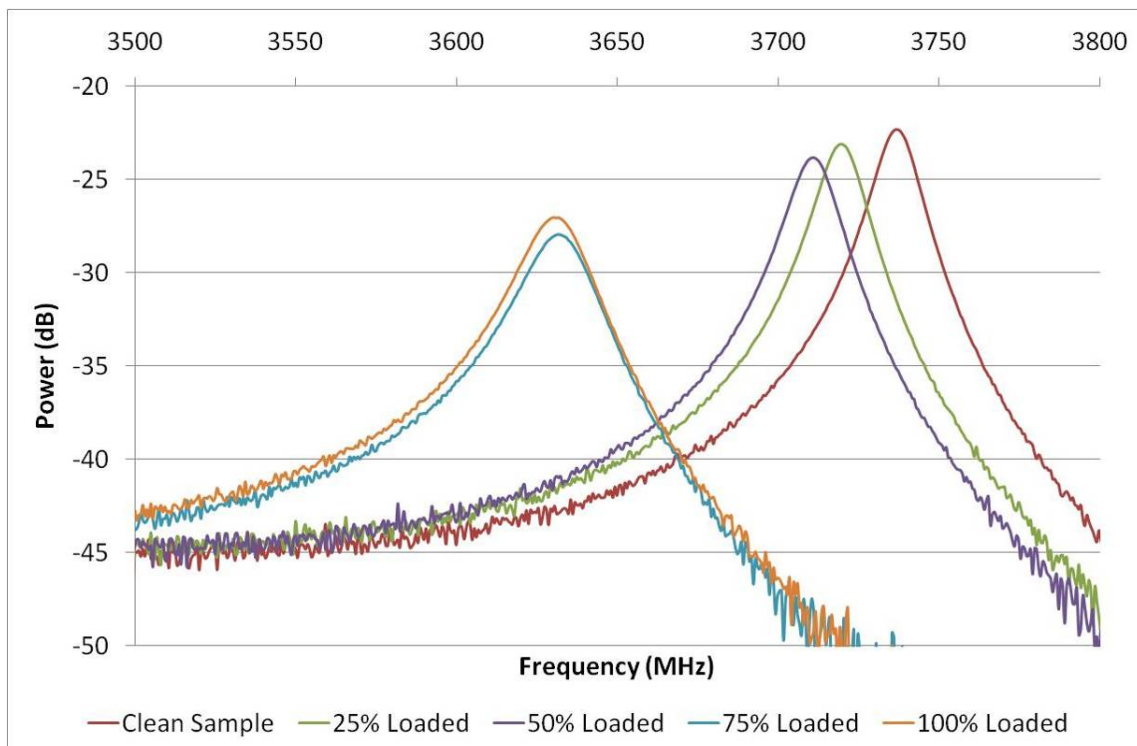


Figure 14. Spectral data for transmitted power in the range 3.5-3.8GHz, showing resonant peak shifts dependant on filter loading.

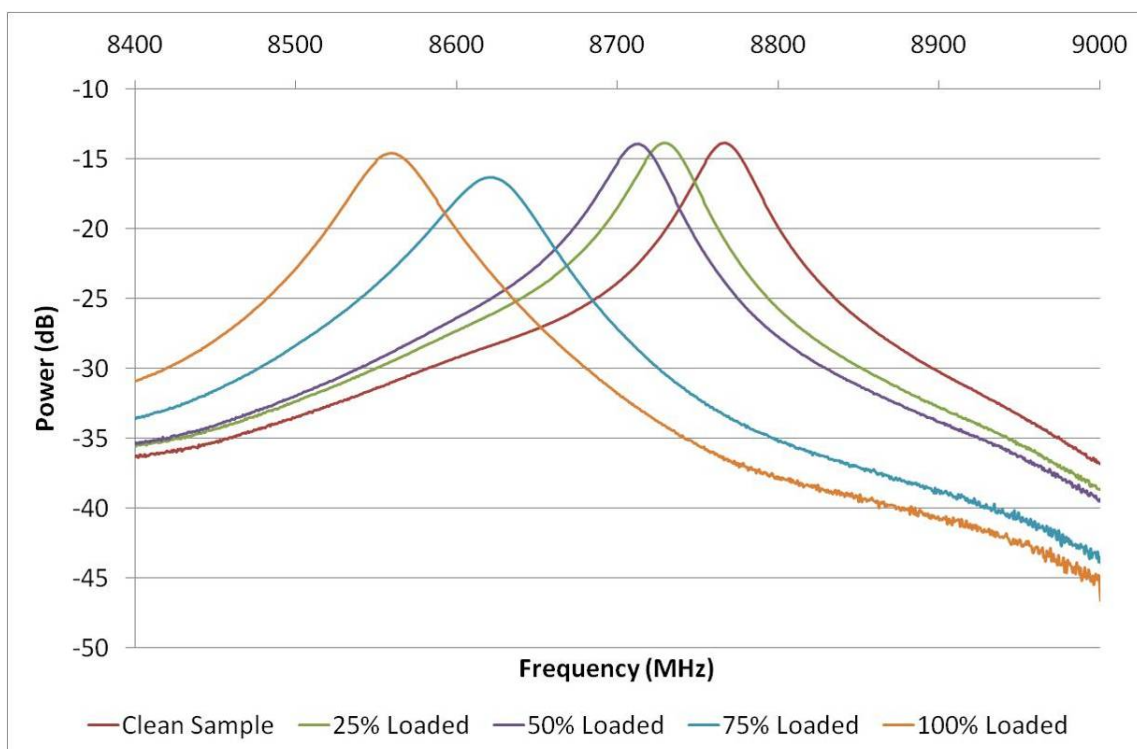


Figure 15. Spectral data for reflected power in the range 8.4-9.0GHz, showing resonant peak shifts dependant on filter loading.

Table 3: Peak information from Figures 10, 11, 13 and 14, indicating the frequency at which peaks occur for each sample, and the change in frequency (Δf) which occurs between each sample.

Sample	Figure 11	Δf	Figure 12	Δf	Figure 14	Δf	Figure 15	Δf
E	3737	--	8765	--	3734	--	8760	--
D	3718	-19	8729	-36	3717	-17	8728	-32
C	3709	-9	8712	-17	3708	-9	8706	-22
B	3632	-77	8621	-91	3622	-86	8615	-91
A	3630	-2	8556	-65	3623	+1	8550	-65

It is clear from the Figures 10-15 and Table 3 that there is change – often significant – occurring in the spectral data as a result of the changing filter load. As expected, this change appears to be represented by shifts in resonant frequency. Results in the region of 8.4-9.0GHz appear to give the most promising results in both reflection and transmission measurements, giving a clearly distinguishable change (17-91MHz) when differently loaded filters are present. It is interesting also that there is no significant change in signal amplitude, and that the samples are ordered such that the clean filter (sample E) gives the highest resonant frequency and the most loaded (sample A) the lowest. This would indicate that the cavity is reacting to the change in ϵ_r ; as ϵ_r changes from that of air toward that of the dust (i.e. increases with higher dust loading), the sensor appears to act as if it has been enlarged, therefore resulting in a lower resonant frequency.

The Q factor at the resonant frequencies is sufficient to distinguish the peaks easily from any background noise, which means that automated load detection would be relatively straight forward. It is possible that the results presented here would display a greater degree of linearity if the dust had not begun to separate itself from the filters with higher loadings (i.e. samples A and B) – Figure 16 shows an example of this separation. This happens because dust at these loadings are not adhered directly to the filter but rather to other dust particles resulting in weak forces keeping them in place.



Figure 16. Separation of dust from sample filters for samples A and B.

V. CONCLUSIONS AND FUTURE WORK

This paper presents a novel technique for the determination of residual filter life using a resonant cavity sensor operating in the regions of 3.5-3.8GHz and 8.4-9.0GHz, where TM_{010} and TM_{020} modes dominate. Experimental work with this cavity clearly shows that artificially loaded filters result in a shift in resonant frequency which corresponds with the amount of dust loaded onto the filter, and therefore the amount of air flow that they would permit in use. The authors perceive that such technology could have applications particularly in situations where filters see periodic rather than continuous use, and slight modification of the sensor design could make it suitable to encapsulating a filter canister from a typical wearable respirator. In addition, the cavity could be used in its present form to test thin filter materials, such as those which might be incorporated into wearable garments.

Future work in this area of research will look to use a greater range of artificially loaded filter samples in order to determine the sensor resolution, accuracy and precision.

REFERENCES

- [1] H. Leibold and J. G. Wilhelm, "Investigations into the penetration and pressure drop of hepa filter media during loading with submicron particle aerosols at high concentrations," *Journal of Aerosol Science*, vol. 22, pp. S773-S776, 1991.
- [2] S. Callé, P. Contal, D. Thomas, D. Bémer, and D. Leclerc, "Description of the clogging and cleaning cycles of filter media," *Powder Technology*, vol. 123, pp. 40-52, 2002.
- [3] H. Alper, "Method for filtering pernicious non-gaseous contaminants from air and benign gases." vol. 1, E. P. Office, Ed., 2005.
- [4] T. Schroth, "New HEPA/ULPA filters for clean-room technology," *Filtration & Separation*, vol. 33, pp. 245-250, 1996.
- [5] S. Callé, D. Bémer, D. Thomas, P. Contal, and D. Leclerc, "Changes in the performances of filter media during clogging and cleaning cycles," *The Annals of Occupational Hygiene*, vol. 45, pp. 115-121, 2001.
- [6] V. J. Novick, P. R. Monson, and P. E. Ellison, "The effect of solid particle mass loading on the pressure drop of HEPA filters," *Journal of Aerosol Science*, vol. 23, pp. 657-665, 1992.
- [7] S. Callé, P. Contal, D. Thomas, D. Bémer, and D. Leclerc, "Evolutions of efficiency and pressure drop of filter media during clogging and cleaning cycles," *Powder Technology*, vol. 128, pp. 213-217, 2002.
- [8] D. Thomas, P. Contal, V. Renaudin, P. Penicot, D. Leclerc, and J. Vendel, "Modelling pressure drop in hepa filters during dynamic filtration," *Journal of Aerosol Science*, vol. 30, pp. 235-246, 1999.
- [9] "The ins and outs of HEPA filters," *Chemical Health and Safety*, vol. 11, pp. 33-33, 2004/4//.
- [10] "Testing of HEPA and ventilation filters," *Filtration & Separation*, vol. 31, pp. 781-781, 1994.
- [11] D. M. Pozar, *Microwave Engineering*, 3rd ed. New York: John Wiley and Sons, 2005.
- [12] Ansoft, "Ansoft HFSS," Cited: 10 January, 2010.